tion and evolution of early life: sulphur isotope clues from Indian Proterozoic basins. *Geol. Mag*., 2010, **147**, 206–218.
10. Clark, S. H. B. and Basu, P. K., Geologic setting and origin of the Mangampeta barite deposit, India. In *Mineral Deposits: Processes to Processing* (eds Stanley, C. J. *et al.*), Balkema, Rotterdam, The Netherlands, 1999, pp. 1085–1088.
11. Crawford, A. R. and Compston, W., The age of the Cuddapah and Kurnool systems, southern India. *J. Geol. Soc. Aust.*, 1973, **19**, 453–464.
12. Shepherd, T. J., Rankin, A. H. and Alderton, D. H. M., *A Practical Guide to Fluid Inclusion Studies*, Blackie, New York, 1985, p. 239.
13. Ostwald, J. and England, B. M., The relationship between euhedral and framboidal pyrite in base-metal sulphide ores. *Mineral. Mag.*, 1979, **43**, 297–300.
14. Ramam, P. K. and Murty, V. N., *Geology of Andhra Pradesh*, Geological Society of India, 1997, p. 245.
15. Thode, H. G., Monster, J. and Dunford, H. B., Sulphur isotope geochemistry. *Geochim. Cosmochim. Acta*, 1961, **25**, 159–174.
16. Allegre, C. J., *Isotope Geology*, Cambridge University Press. 2008, p. 512.
17. Seal, R. R., Sulfur isotope geochemistry of sulfide minerals. *Rev. Mineral. Geochem.*, 2006, **61**, 633–677.

ACKNOWLEDGEMENTS. We thank the anonymous reviewers whose in-depth reviews have been helpful in improving the manuscript. We also thank R. Ramesh who helped us improve the language of the manuscript.

Received 12 December 2012; revised accepted 15 May 2013

Field evaluation of 3D geo-electrical resistivity imaging for environmental and engineering studies using parallel 2D profiles

A. P. Aizebeokhai[1] and V. S. Singh[2,*]

[1]Department of Physics, Covenant University, Ota, Nigeria
[2]CSIR-National Geophysical Research Institute, Hyderabad 500 007, India

Eight parallel two-dimensional (2D) geo-electrical resistivity profiles were generated in hard-rock (Pulivendla) area of Andhra Pradesh, India using a Lund imaging multi-electrode system adopting Wenner array. The aim of the survey was to experimentally evaluate the effectiveness of using parallel 2D profiles for three-dimensional (3D) geo-electrical resistivity imaging for better understanding of aquifer geometry and its characteristics. The observed 2D apparent resistivity data were independently inverted, and then collated to 3D data set. The inversion of the resulting 3D data set was carried out using a full 3D inversion code. The 3D inverse model of resistivity images obtained are presented as horizontal depth slices. The 2D images extracted from 3D inverse models showed no distortions that are observed in 2D models obtained by 2D inversion. The 3D inverse model resistivity appears to be more realistic, considering the hydrogeology of the area. The unusually high resistivity values observed in the 2D inverse models were not observed in the 3D inverse models. The very low near-surface inverse model resistivity observed is thought to be structurally influenced. The results, which are consistent with numerical evaluation, show that high resolution 3D geoelectrical resistivity imaging can be successfully conducted using parallel 2D profiles if appropriate survey parameters are carefully chosen.

Keywords: Field evaluation, 2D and 3D imaging, 3D inversion, parallel 2D profiles, resistivity survey.

GEOELECTRICAL resistivity imaging has been used to address a wide variety of hydrological, environmental and engineering problems. Subsurface geology in many hydrological, environmental and engineering sites is often subtly heterogeneous and on multi-scale, such that the variations of the subsurface properties can be very rapid and erratic. Two-dimensional (2D) geo-electrical resistivity imaging is often used to investigate areas with such complex subsurface geology[1–5]. In 2D resistivity surveys, subsurface resistivity is usually assumed to vary vertically with depth and laterally along the profile, but constant in the direction perpendicular to the profile. However, subsurface features are inherently three-dimensional (3D). Thus, the 2D assumption is commonly violated. The violation of the 2D assumption often leads to out-of-plane resistivity anomaly in the 2D inverse models and this could be misleading in the interpretation of subsurface features[6,7]. Thus, a 3D geo-electrical resistivity imaging which allows resistivity variation in all possible directions should give more accurate and reliable inverse models of the subsurface resistivity. 3D geo-electrical resistivity imaging can be used to characterize the heterogeneity of aquifer system, which allows for better understanding of groundwater flow and management. In addition, 3D geo-electrical resistivity imaging can be used to plan monitoring of groundwater flow at the sites of more focused studies, such as, nuclear installations, landfill sites and waste disposal sites which often requires 3D definition of the aquifer geometry and characterization. It has also been used in archaeological studies, treasure hunt, detection of underground leakages, etc.

The techniques for conducting 3D resistivity surveys have been presented by Loke and Barker[8]. Square and rectangular grids of electrodes with constant electrode spacing in both *x*- and *y*-directions are commonly used[8–12]. Each electrode in the grid is in turn used as the current electrode while the potential difference is measured at all other electrode positions. However these techniques,

*For correspondence. (e-mail: vssingh77@hotmail.com)

which allow the measurements of complete 3D data sets, are usually impractical due to the large length of cables and the number of electrodes, as also the site geometry one commonly faces in most practical surveys. For a survey involving large grids of electrodes, the number of possible electrode permutations for the measurements will be very large. Thus, the measurement of complete 3D data sets using the square or rectangular grids of electrodes is time-consuming and cumbersome.

Several surveying techniques have been adopted to reduce the number of data measurements as well as the time and effort required for 3D geoelectrical resistivity field surveys. These techniques include cross-diagonal surveying technique that allows resistivity measurements to be made only at the electrodes along the *x*-axis, *y*-axis and 45-degrees diagonal lines[8], orthogonal 2D surveying technique[5–7,13] in which apparent resistivity measurements of orthogonal 2D lines are collated to 3D data set, and parallel 2D surveying techniques that allows the collation of apparent resistivity measurements made in parallel 2D profiles to 3D data set[14,15].

The orthogonal and parallel 2D surveying techniques, which allow flexible survey design, choice of array and easy adaptability to data acquisition systems, requires that appropriate inter-line spacing between the 2D profiles be chosen to obtain high resolution 3D resistivity images. Numerical evaluation of the parallel 2D resistivity techniques shows that the technique is efficient, cost-effective and fast for 3D resistivity surveys, especially in areas with complex subsurface geology[14,15]. The main objective of the present study is experimental evaluation of the practicability and effectiveness of using parallel set of 2D profiles for 3D geoelectrical resistivity imaging. The survey has been conducted in a hard rock area near Pulivendla, Andhra Pradesh, Southern India (14.4167°N, 78.2333°E). The study also aimed at determining the soil salinity of the site and its impact on the shallow groundwater system.

In the area of study, the Proterozoic Cuddapah Supergroup overlies Archean Crystalline rock basement[16]. The rocks of the Cuddapah Supergroup overlie the basement with strong angular unconformity. The Cuddapah Supergroup (Figure 1) consists of weakly metamorphosed sandstones, shale, dolomite and limestones which are the main rock[17]. They occur in a dissected plateau with parallel ridges.

The general climate of the region is semi-arid. The temperature gradually rises from January and reaches its maximum (42°C) in April and decreases gradually from May and reaches a minimum in December (20°C). Relative humidity shows that seasonal variations generally fluctuate with rainfall and temperature apart from the diurnal variations. The relative humidity is higher (57–75) during monsoon and winter as a result of the increase in rainfall and decrease in temperature. Similarly, relative humidity is less in summer due to the combined effect of high temperature and precipitation. Average annual rainfall is 703 mm, with the range from 501 to 1064 mm.

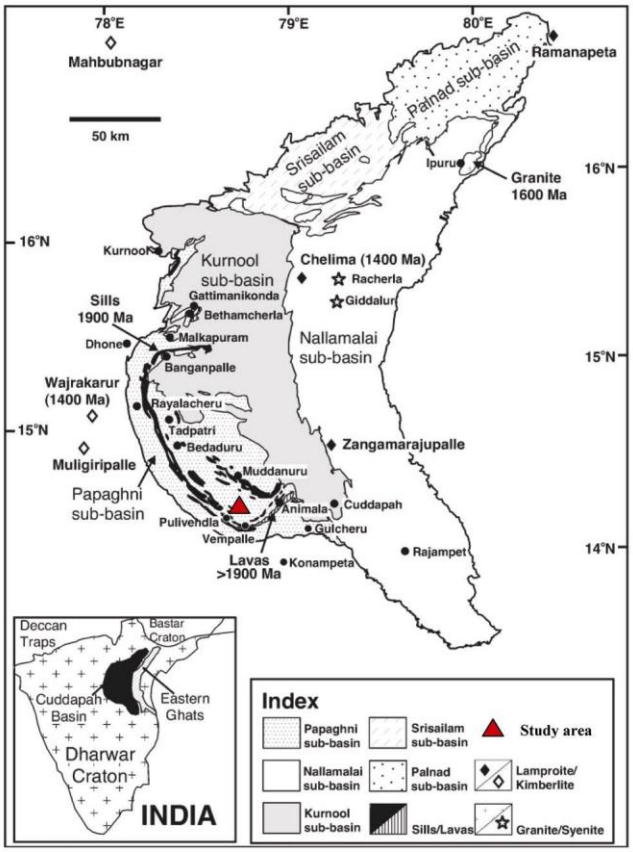

Figure 1. Geological map of Cuddapah basin[22] showing the study area near Pulivendla.

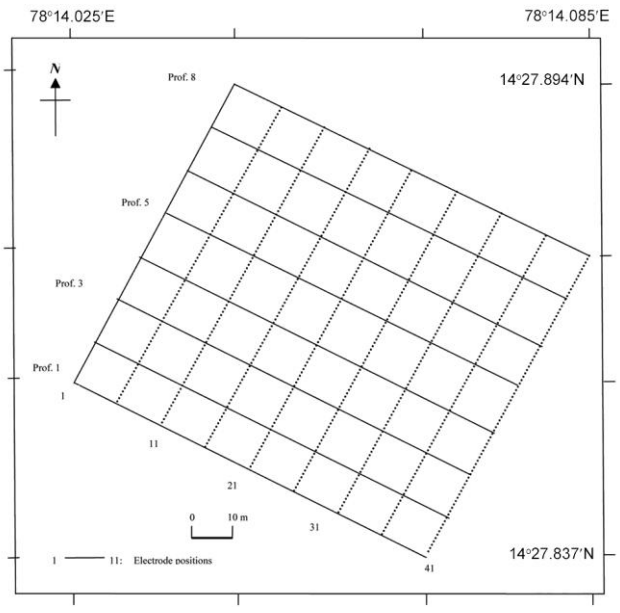

Figure 2. Geoelectrical resistivity survey plan showing the locations of 2D traverses.

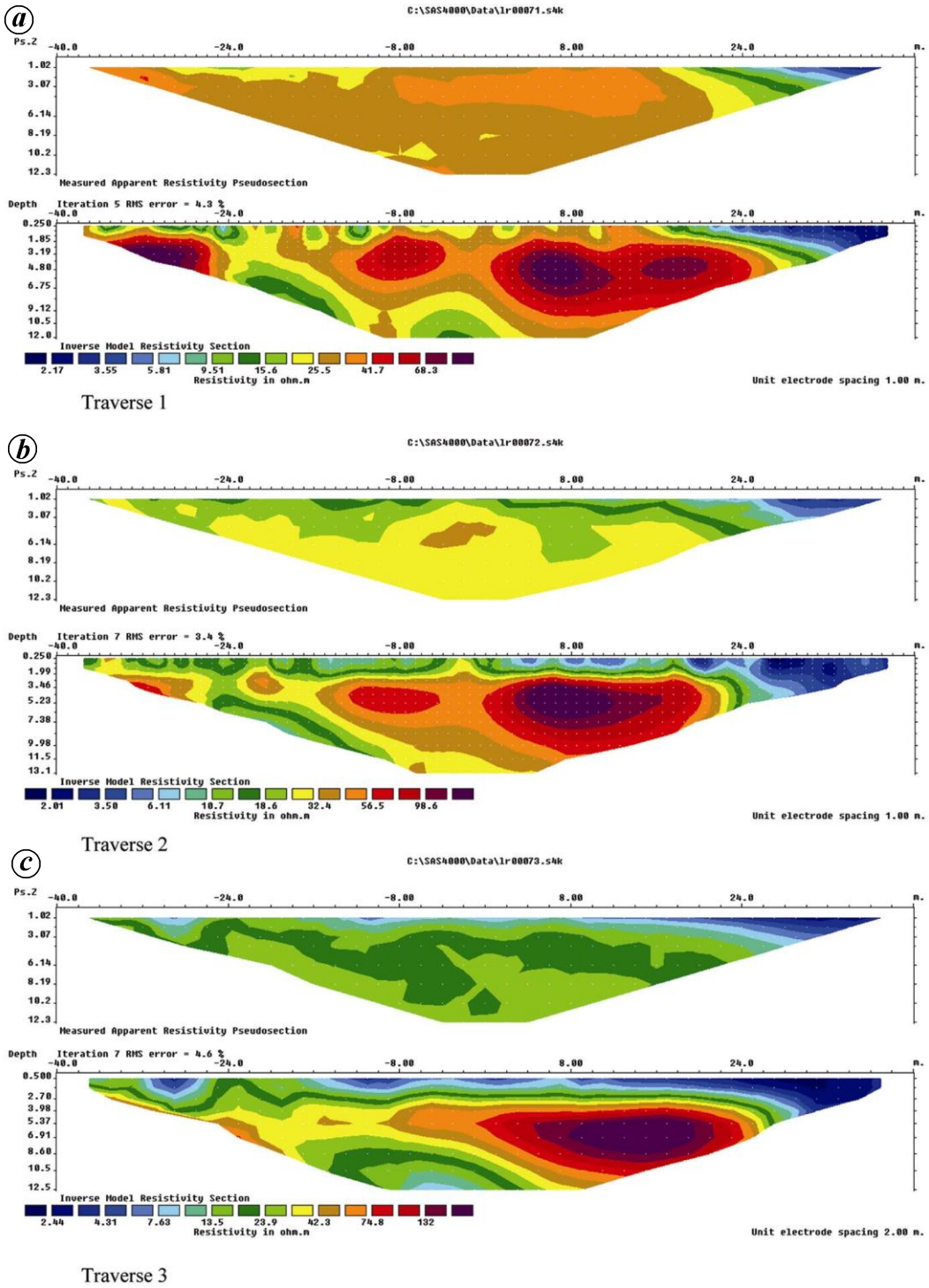

Figure 3. 2D smoothness constrained inverse model resistivity sections and measured apparent resistivity pseudosections for: (***a***) Traverse 1; (***b***) Traverse 2; (***c***) Traverse 3.

Usually, the region receives its first pre-monsoon showers in May; however, the occurrence of this event is erratic. The intensity and amount of rainfall is unpredictable during the southwest monsoon period (June to September); and the highest rainfall occurs during the northeast monsoon period (October and November). The period between January and May is the main dry season and receives some rainfall due to convections or winter cyclonic disturbances.

Groundwater occurs in all the geological formations in the basin. The occurrence and behaviour of groundwater is controlled by geological, structural and climatological

factors, which together influence the groundwater dynamic system. Two main groups of rocks, from the groundwater point of view, are known in the basin. These are the consolidated rocks comprising quartzites, shales, limestones, granites and granite gneisses; and the unconsolidated formations consisting of alluvium. The aquifer system in consolidated rocks is highly disconnected and varies widely. Groundwater occurs under water table conditions in weathered portion of the formation and thickness of the weathered profile is about 10 m below ground level[18].

Eight parallel 2D geo-electrical resistivity profiles (Figure 2) were conducted in February (post-monsoon) using SAS1000 Lund imaging multi-electrode system which has one input channel. The survey was conducted using a layout of 41 electrodes at 2.0 m spacing (Figure 2), giving a total length of 80.0 m for each of the 2D profiles which were oriented in S50°E–N50°W direction. Inter-line spacing of 10.0 m (five times the minimum electrode separation) between each of the 2D profiles was used in the survey; thus giving electrode grid size of 41×8 with a total survey area of 80 m × 70 m, corresponding to 41 electrodes in the *x*-direction and 8 electrodes in the *y*-direction respectively. The survey area was more or less flat with a maximum elevation difference of less than 0.1 m; hence elevation corrections were not incorporated to the field measurements.

The conventional Wenner array was used for data collection in all 2D profiles. Two cables, each with 21 electrode take-outs were used for the survey; the last electrode take-out of the first cable and the first electrode take-out of the second cable were overlapped at the midpoint of each survey line. The cables were connected to an automated electrode selector which scanned all the electrodes to ensure that they were all connected to the electrode cables and had good contact with the ground. Electrode positions were watered so as to ensure good contact between the ground and electrodes. The apparent resistivity readings were written on the disk file in the imaging system and were then transferred to an external PC after field observations. A total of 190 datum points were read in each of the 2D profiles.

The observed apparent resistivity data for each of the 2D profiles were processed with RES2DINV computer code[8]. The RES2DINV computer program uses a nonlinear optimization technique which automatically determines a 2D resistivity model of the subsurface for the input apparent resistivity data[1,8]. The program divides the subsurface into a number of rectangular blocks according to the spread of the observed data. Least-squares inversion with standard least-squares constraint which attempt to minimize the square of the difference between the observed and the calculated apparent resistivity values was used to invert all the 2D traverses. Smoothness constraint was applied to the model perturbation vector only and appropriate damping factors were selected using trial and error methods. Apparent resistivity datum points with greater than 50% root mean square (RMS) errors were eliminated from the 2D data set before final inversion. The inverted model sections and measured apparent resistivity pseudosections for the 2D profiles are given in Figures 3 to 5.

The observed apparent resistivity data for the eight parallel 2D profiles were then collated to 3D data set, after isolating datum points with RMS error greater than 50% from the individual 2D data set. The 2D data sets were collated on a 3D grid of 41×8 electrodes with a density of 1520 data points. The 3D grid corresponds to a separation of 2 m on the *x*-axis and 10 m on the *y*-axis, since the profiles were separated by inter-line spacing of five times the minimum electrode spacing. The inversion of the 3D data set collated was carried out using RES3DINV, a full 3D inversion code, which automatically determines a 3D inverse model of resistivity distribution using apparent resistivity data obtained from a 3D resistivity imaging survey[9,19]. The process of inversion involves consideration subsurface layer as number of small rectangular prism. The resistivity values of these prisms are determined so as to minimize the difference between calculated and observed apparent resistivity values. Ideally, the electrodes used for such a survey are arranged in squares or rectangular grids. The inversion routine used by the RES3DINV program is based on the smoothness constrained least-squares method[20,21], as in RES2DINV for 2D inversion, though a robust inversion can also be implemented. The program allows users to adjust the damping factor and the flatness filters in the equation below to suit the data set being inverted.

$$\{J^{\mathrm{T}}J + \mu(f_x f_x^{\mathrm{T}} + f_z f_z^{\mathrm{T}})\}d = J^{\mathrm{T}}g, \tag{1}$$

where f_x is the horizontal flatness, f_z the vertical flatness, μ the damping factor, J the Jacobian matrix of partial derivatives, d the model perturbation vector, g the discrepancy vector which contains the differences between the logarithms of the measured and calculated apparent resistivity values, and J^{T} is the transpose of J.

The smoothness constrained least-squares inversion method implementing the finite difference method was used in inverting the data. Initial damping factor of 0.15 and a minimum damping factor of 0.011, and standard Gauss–Newton optimization method were used in the inversion. After each iterating process, the inversion subroutine generally reduced the damping factor used; a minimum limit (one-tenth of the value of the initial damping factor used) was set to stabilize the inversion process. The damping factor was increased by a factor of 1.050 for each deeper layer and optimized so as to reduce the number of iterations the inversion code required for convergence. In order to determine the 3D distribution of the model resistivity values from the distribution of

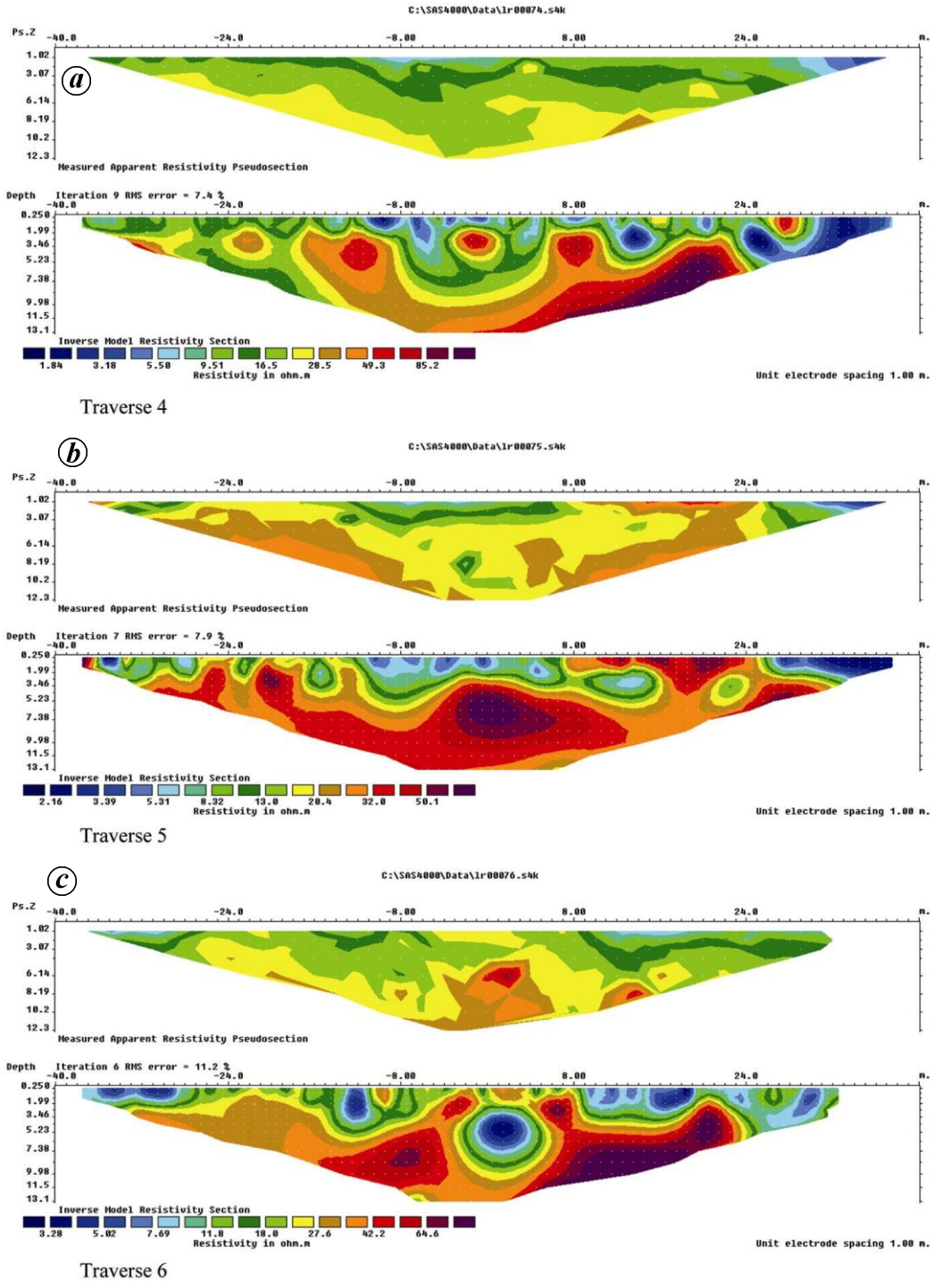

Figure 4. 2D smoothness constrained inverse model resistivity sections and measured apparent resistivity pseudosections for: (***a***) Traverse 4; (***b***) Traverse 5; (***c***) Traverse 6.

apparent resistivity values, the subsurface was subdivided into a number of small rectangular blocks.

The program defunct for the first layer thickness based on the maximum depth of investigation of the array was used and was increased by 1.15 (15%) for subsequent layers since resolution decreases with depth. Homogeneous earth model was used as the initial model for inversion. Also, four-nodes were used between adjacent electrodes in the finite difference so as to significantly increase the accuracy of the 3D inversion model. Potential values were normalized during the inversion. The inversion converged with a RMS error of 14.0% after five iterations. The 3D inversion models are presented as horizontal depth slices in Figure 6 and 2D images

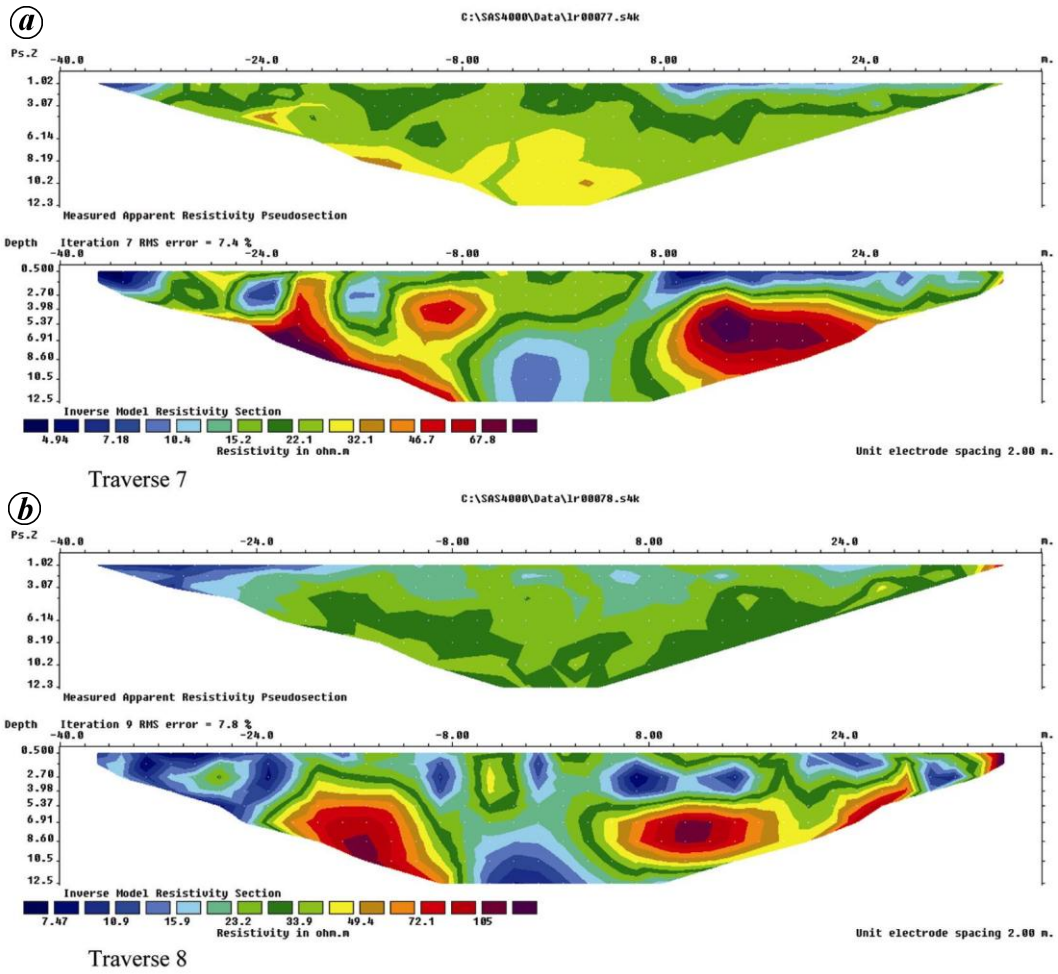

Figure 5. 2D smoothness constrained inverse model resistivity sections and measured apparent resistivity pseudosections for: (***a***) Traverse 7; (***b***) Traverse 8.

extracted from the 3D inversion models, which are compared directly with the 2D inversion models, are presented in Figure 7.

The 2D inverse resistivity models presented in Figures 3 to 5 generally show low model resistivity values that range from a minimum of about 2 Ωm to a maximum of about 150 Ωm. There is a reasonable agreement and correlation of the inverse model resistivity sections among all the 2D profiles presented. The top soil is characterized with very low model resistivity values ranging from about 2 to 8 Ωm with a model layer thickness of about 1.5 Ωm. This high conductivity layer is largely composed of loamy silt with increased salinity due to the application of fertilizers on the soil for crop cultivation and alteration of the soil density due to tillage. A relatively higher resistive layer corresponding to fractured shale (Rangarajan, R., pers. commun., 2013) underlies the top soil with inverse model resistivity values ranging from about 65 Ωm to 150 Ωm. The high resistivity of more than 100 Ωm as observed in traverse 2 and 3 seems to be more than expected. The maximum depth of investigation for the 2D inverse models is 12.5 m on an average.

The 3D inverse model resistivity images obtained are presented as horizontal depth slices in Figure 6. The inverse model resistivity values range from a minimum of about 21 Ωm, which is consistent with that obtained from the 2D inverse models, to a maximum of about 75 Ωm. The inverse model resistivity observed in the 3D inversion indicates that the abnormally high model resistivity values observed in the 2D inversion images has been eliminated. The study area is occupied by weathered zone underlain by fractured shale (Rangarajan, R., pers. commun., 2013). The abnormally high inverse model resistivity in the 2D inversion images are thought to be out-of-plane resistivity anomaly in the 2D inverse models. This may be due to the violation of the 2D assumption in characterizing 3D effects on the resulting 2D inverse model images[6,7]. The effective depth of investigation, as observed in the 3D inverse models, is greater than 13.7 m which is higher than that attained in the 2D inversion of the collated profiles. The observed 3D inverse model images suggest that the very low near-surface inverse model resistivity in the study area may be principally due to the near-surface lithology other than increased salinity.

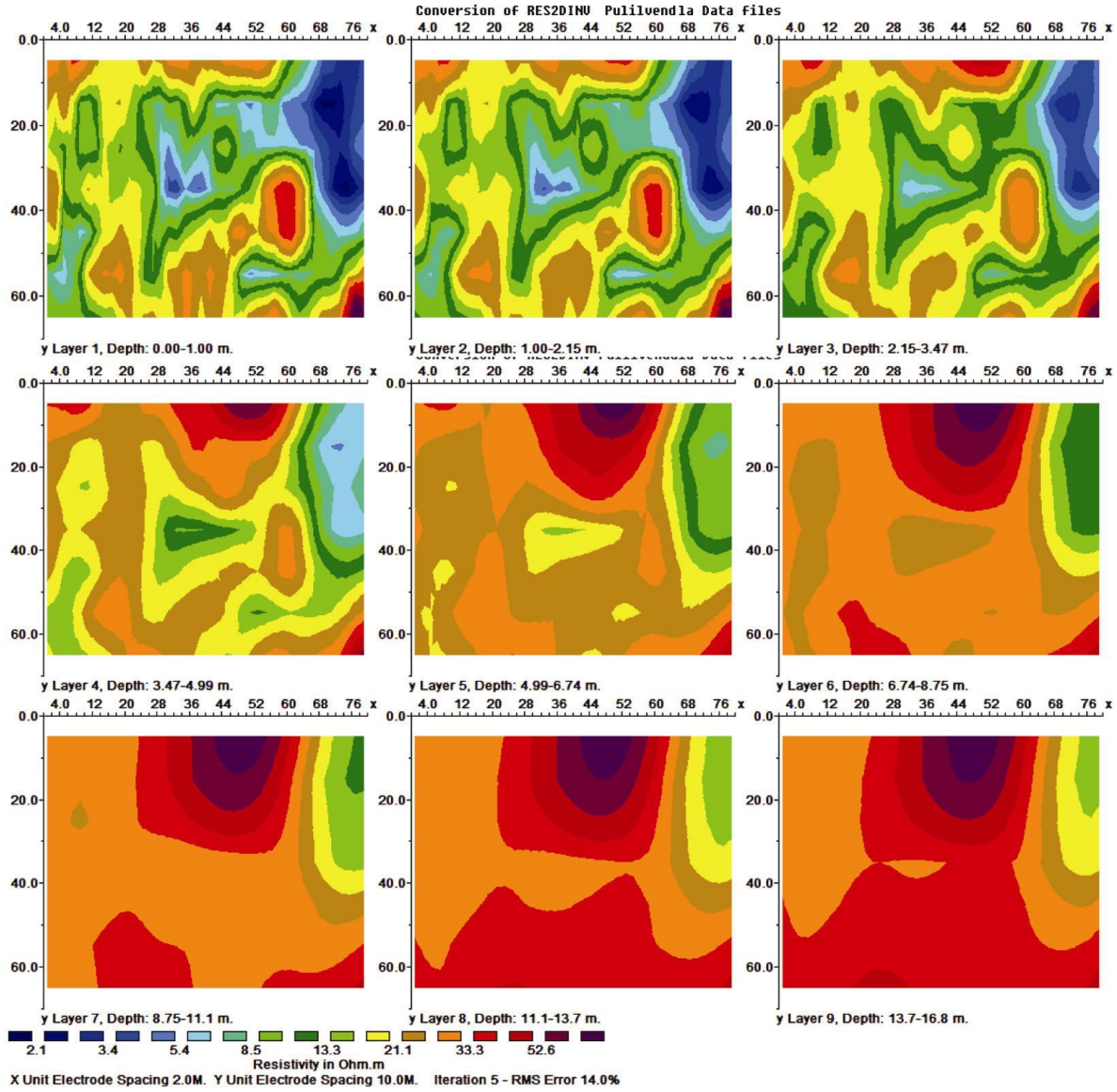

Figure 6. Horizontal depth slices obtained from the 3D inversion of eight parallel 2D profiles using smoothness constrained least-squares inversion, Pulivendla, India.

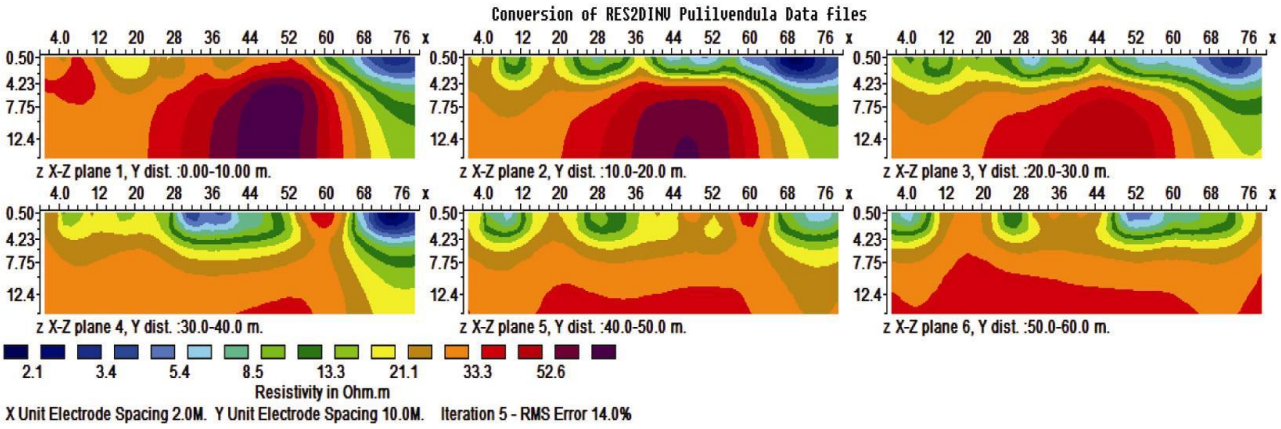

Figure 7. Extracted 2D vertical *x*–*z* slices from the 3D inversion models shown above (smoothness constrained least-squares method).

The high RMS error of 14.0% observed in the 3D inversion model is partly attributed to the differences in the error characteristics of the parallel 2D data sets collated to the 3D data set on the one hand. The combination of the different error characteristics of the 2D data sets can complicate the error characteristic of the resulting 3D data set. Other factors that may be responsible for the high RMS error in the 3D inverse model include the inter-line spacing relative to the 2D profiles to the minimum electrode separation used for the survey as well as the 3D inversion code used for data inversion. The inversion code is specifically designed for 3D data acquired using square or rectangular grid of electrodes. The RMS error can be greatly reduced if the inter-line spacing relative to the minimum electrode separation is reduced as this will increase the data density in the 3D data set, and consequently increase inverse model resolution.

The 2D images in the x–z plane extracted from the 3D inversion models, where x is the direction of the 2D profiles and z is depth, are shown in Figure 7. These 2D images are extracted at the mid-point between two adjacent 2D profiles so that the inverse model results can be directly compared. A direct comparison between the observed 2D inverse models and the extracted 2D inverse models shows that the 3D inverse model resistivity is more realistic and contains fewer artefacts than the inverse model resistivity obtained in the 2D inversion of the same data set. The 2D model images extracted from 3D inverse models show evidence of vertical structures with high resistivity anomaly in the investigated site, and this could not be easily inferred from the 2D inversion images for the same data set. This may be due to the inability of 2D imaging to effectively map 3D features. Thus, 3D geoelectrical resistivity imaging/inversion is superior to the conventional 2D imaging/inversion, especially in complex heterogeneous subsurface.

The effects of grid orientation in the 3D inversion images obtained are minimal, suggesting that 3D geoelectrical resistivity survey in which the 3D data set is collated from closely spaced parallel 2D profiles can produce good quality and high resolution 3D images. The 3D geoelectrical resistivity inverse models obtained in this study are considered reasonable and realistic. These results agree largely with the ones obtained from numerical evaluation of 3D data acquisitions using parallel 2D profiles[14,15]. Although inter-line spacing of five times the minimum electrode spacing between the parallel 2D profiles was used for this study, results obtained from numerical evaluation indicate that, the inter-line spacing of four times the minimum electrode spacing or less would yield good quality and high resolution 3D inversion models[14,15]. Larger inter-line spacing relative to the minimum electrode separation would produce 3D inversion models that are prone to near-surface artefacts and grid orientation effects and could be misleading for interpretation. The inter-line spacing relative to the minimum electrode separation should be as small as possible within practical limits; ideally, it should be equal to the minimum electrode spacing. This is often not practicable due to the cost of the survey and the desire to speed up field procedures. Thus, good quality and high resolution 3D geoelectrical resistivity imaging can be successfully conducted using parallel 2D profiles if appropriate inter-line spacing relative to the minimum electrode separation is carefully chosen.

A 3D geoelectrical resistivity imaging has been successfully conducted by collating apparent resistivity data of parallel 2D profiles to a 3D data set. The 3D data set collated was successfully inverted using RES3DINV computer program, which is a full 3D inversion code designed for 3D data set collected using a square or rectangular grid of electrodes. The unusually high inverse model resistivity values observed in the 2D models are not observed in the 3D inverse models. These abnormally high resistivity values in the 2D inverse models are attributed to 3D effects of subsurface features on the 2D data sets. The very low surface inverse resistivity models in the near-surface are thought to be mainly due to the near-surface lithology. The effect of increased salinity and tillage on the resistivity models and the consequent impacts on the shallow groundwater system is therefore minimal.

Thus, good quality and high resolution 3D geo-electrical resistivity imaging can be successfully conducted using parallel 2D profiles if appropriate inter-line spacing relative to the minimum electrode separation is carefully chosen. Ideally, the inter-line spacing should be equal to the minimum electrode separation; but this may not be practicable due to cost and time required for the survey. A compromise is often made between speed and resolution. The smaller the inter-line spacing relative to the minimum electrode separation between the parallel 2D profiles, the better the quality and resolution of the 3D model inversion images that would be obtained. Hence, the acquisition of 3D geoelectrical resistivity data using parallel 2D profiles is fast, efficient and cost-effective, and can yield high resolution 3D inverse models if appropriate survey parameters are used.

1. Griffiths, D. H. and Barker, R. D., Two-dimensional resistivity imaging and modelling in areas of complex geology. *J. Appl. Geophys.*, 1993, **29**, 211–226.
2. Dahlin, T. and Loke, M. H., Resolution of 2D Wenner resistivity imaging as assessed by numerical modelling. *J. Appl. Geophys.*, 1998, **38**, 237–248.
3. Olayinka, A. I. and Yaramanci, U., Choice of the best model in 2-D geoelectrical imaging: case study from a waste dump site. *Eur. J. Environ. Eng. Geophys.*, 1999, **3**, 221–244.
4. Amidu, S. A. and Olayinka, A. I., Environmental assessment of sewage disposal systems using 2D electrical resistivity imaging and geochemical analysis: A case study from Ibadan, Southwestern Nigeria. *Environ. Eng. Geosci.*, 2006, **7**, 261–272.
5. Aizebeokhai, A. P., Olayinka, A. I. and Singh, V. S., Application of 2D and 3D geoelectrical resistivity imaging for engineering site

investigation in a crystalline basement terrain, southwestern Nigeria. *J. Environ. Earth Sci.*, 2010, **61**, 1481–1492.
6. Bentley, L. R. and Gharibi, M., Two- and three-dimensional electrical resistivity imaging at a heterogeneous site. *Geophysics*, 2004, **69**, 674–680.
7. Gharibi, M. and Bentley, L. R., Resolution of 3D electrical resistivity images from inversion of 2D orthogonal lines. *J. Environ. Eng. Geophys.*, 2005, **10**, 339–349.
8. Loke, M. H. and Barker, R. D., Rapid least-squares inversion of apparent resistivity pseudosections by a quasi-Newton method. *Geophys. Prospect*., 1996, **44**, 131–152.
9. Li, Y. and Oldenburg, D. W., Inversion of 3D DC resistivity data using an approximate inverse mapping. *Geophys. J. Int*., 1994, **116**, 527–537.
10. Park, S., Fluid migration in the vadose zone from 3D inversion of resistivity monitoring data. *Geophysics*, 1998, **63**, 41–51.
11. Chambers, J. E., Ogilvy, R. D., Meldrum, P. I. and Nissen, J., 3D electrical resistivity imaging of buried oil-tar contaminated waste deposits. *Eur. J. Environ. Eng. Geophys.*, 1999, **4**, 3–15.
12. Ogilvy, R., Meldrum, P. and Chambers, J., Imaging of industrial waste deposits and buried quarry geometry by 3D tomography. *Eur. J. Environ. Eng. Geophys.*, 1999, **3**, 103–113.
13. Aizebeokhai, A. P., Olayinka, A. I. and Singh, V. S., Numerical evaluation of 3D geoelectrical resistivity imaging for environmental and engineering investigations using orthogonal 2D profiles. *SEG Expanded Abstr.*, 2009, **28**, 1440–1444.
14. Aizebeokhai, A. P. and Olayinka, A. I., Anomaly effects of arrays for 3D geoelectrical resistivity imaging using orthogonal or parallel 2D profiles. *Afr. J. Environ. Sci. Technol.*, 2010, **4**, 446–454.
15. Aizebeokhai, A. P., Olayinka, A. I., Singh, V. S. and Uhuegbu, C. C., Effectiveness of 3D geoelectrical resistivity imaging using parallel 2D profiles. *Curr. Sci*., 2011, **101**, 1036–1052.
16. Nagaraja Rao, B. K., Rajurkar, S. T., Ramalingaswamy, G. and Ravindra Babu, B., Stratigraphy, structure and evolution of Cuddapah basin. *Geol. Soc. India Mem*., 1987, **6**, 33–86.
17. Jeyagopal, A. V., Raju, R. D., Maithani, P. B. and Chaki, A., Cyclic sedimentation and classification of the Papaghni Group of sediments, Cuddapah basin, Andhra Pradesh. *J. Geol. Soc. India*, 2008, **71**, 363–370.
18. Reddy, G. R. C., Ground water information Kadapa district, Andhra Pradesh, Southern Region, Central Groundwater Board, 2007, 1–47.
19. White, R. M. S., Collins, S., Denne, R., Hee, R. and Brown, P., A new survey design for 3D IP modelling at Copper hill. *Explor. Geophys.*, 2001, **32**, 152–155.
20. deGroot-Hedlin, C. and Constable, S. C., Occam's inversion to generate smooth two-dimensional models from magnetotelluric data. *Geophysics*, 1990, **55**, 1613–1624.
21. Sasaki, Y., Resolution of resistivity tomography inferred from numerical simulation. *Geophys. Prospect.*, 1992, **40**, 453–464.
22. Nagaraja Rao, B. K. and Ramalingaswamy, G., Some new thoughts on stratigraphy of Cuddapah Supergroup. *Seminar on Kaladgi-Badami, Bhima and Cuddapah Supergroup*, Mysore, India, 1976, pp. 17–20.

ACKNOWLEDGEMENTS. The Third World Academy of Science (TWAS), Italy in collaboration with the Council of Scientific and Industrial Research (CSIR), India acknowledged for providing Fellowship to first author for this study at the National Geophysical Research Institute (NGRI), Hyderabad, India. The second author thanks CSIR for Emeritus fellowship. Thanks are also due to Dr R. Rangarajan, Chief Scientist, NGRI and his colleagues for discussions and necessary help during field work.

Received 20 September 2012; revised accepted 13 June 2013

Quantification of gas hydrate and free gas in the Andaman offshore from downhole data

Maheswar Ojha* and Kalachand Sain

CSIR-National Geophysical Research Institute, Uppal Road, Hyderabad 500 007, India

Under Expedition-01 of Indian National Gas Hydrate Programme (NGHP Exp-01), drilling/coring was done in 2006 at one site in the Andaman Sea, where the base of gas hydrate stability, coinciding with the bottom simulating reflector (BSR) on seismic section, was observed at 610 m below sea floor (mbsf) with water depth of 1344 m. We estimate the saturation of gas hydrate and free gas by applying rock physics theories to downhole sonic velocity, and compare the results with the resistivity and chlorinity data. The result matches well with the pressure core data. Although the average saturation of gas hydrate is only 5% of pore volume (or 3% of sediment volume), the total amount of gas in the form of gas hydrate is about 1570.8 cubic metre within the sediментary column of 308 m above the BSR. The average concentration of free gas is estimated as ~1.4% of the pore volume within the sedimentary column of 80 m below the BSR.

Keywords: National Gas Hydrate Programme, quantification, rock physics.

ONE of the world's deepest and thickest gas hydrate-bearing zone was identified on the seismic data[1]. Drilling and coring were carried out at one site in the Andaman Sea during Expedition 01 of the Indian National Gas Hydrate Programme (NGHP Exp-01) for validating the ground truth of gas hydrate as inferred from seismic data (Figure 1). The Site NGHP-01-17 is located at 10°45.1912′N, 93°6.7365′E in the Andaman Sea, where coring along with wire line sonic, gamma ray, density and resistivity logging were carried out through sediments up to 691.6 m below the sea floor (mbsf) with water depth of ~1344 m (ref. 1). Very low geothermal gradient (19 ± 2°C per km) and high rate of sedimentation (~5.6 cm/kyr) led to thick gas hydrate zone in this area. The infrared (IR) thermal and porewater Cl^- anomalies at site 17 indicate gas hydrate within the ash-rich sediments between 250 to 608 mbsf where the bottom stimulating reflector (BSR), representing the base of gas hydrate stability field, has been observed on seismic section along a line passing through site 17 (ref. 1). Due to bad hole condition, good quality sonic velocity is available from ~300 mbsf, which has been used here to estimate the saturation of gas hydrate and free gas across the BSR. We

*For correspondence. (e-mail: maheswar_ojha@yahoo.com)